Early-onset liver mtDNA depletion and late-onset proteinuric nephropathy in *Mpv17 knockout* mice

Carlo Viscomi[1], Antonella Spinazzola[1], Marco Maggioni[3], Erika Fernandez-Vizarra[1], Valeria Massa[1], Claudio Pagano[4], Roberto Vettor[4], Marina Mora[2] and Massimo Zeviani[1,*]

[1]Unit of Molecular Neurogenetics – Pierfranco and Luisa Mariani Center for the Study of Mitochondrial Disorders in Children and [2]Unit of Neuromuscular Diseases, IRCCS Foundation Neurological Institute 'C. Besta', Milan, Italy, [3]Service of Pathology, San Paolo University Hospital, Milan, Italy and [4]Department of Medical and Surgical Sciences, University of Padova School of Medicine, Padova, Italy

In humans, *MPV17* mutations are responsible for severe mitochondrial depletion syndrome, mainly affecting the liver and the nervous system. To gain insight into physiopathology of *MPV17*-related disease, we investigated an available *Mpv17 knockout* animal model. We found severe mtDNA depletion in liver and, albeit to a lesser extent, in skeletal muscle, whereas hardly any depletion was detected in brain and kidney, up to 1 year after birth. Mouse embryonic fibroblasts did show mtDNA depletion, but only after several culturing passages, or in a serumless culturing medium. In spite of severe mtDNA depletion, only moderate decrease in respiratory chain enzymatic activities, and mild cytoarchitectural alterations, were observed in the *Mpv17*$^{-/-}$ livers, but neither cirrhosis nor failure ever occurred in this organ at any age. The mtDNA transcription rate was markedly increased in liver, which could contribute to compensate the severe mtDNA depletion. This phenomenon was associated with specific downregulation of Mterf1, a negative modulator of mtDNA transcription. The most relevant clinical features involved skin, inner ear and kidney. The coat of the *Mpv17*$^{-/-}$ mice turned gray early in adulthood, and 18-month or older mice developed focal segmental glomerulosclerosis (FSGS) with massive proteinuria. Concomitant degeneration of cochlear sensory epithelia was reported as well. These symptoms were associated with significantly shorter lifespan. Coincidental with the onset of FSGS, there was hardly any mtDNA left in the glomerular tufts. These results demonstrate that *Mpv17* controls mtDNA copy number by a highly tissue- and possibly cytotype-specific mechanism.

INTRODUCTION

The term mitochondrial DNA depletion syndrome (MDS) designates a group of autosomal recessive traits characterized by low mtDNA copy number in specific tissues (1).

Three clinical presentations are known: myopathic, encephalomyopathic and hepatocerebral. This condition is genetically heterogeneous; in ∼80% of the cases the gene remains elusive. In the remaining 20%, several disease genes have been identified, that are responsible for different clinical presentations (2). For instance, mutations in thymidine kinase 2 (TK2) (3) and deoxyguanosine kinase (dGK) (4),

two enzymes involved in deoxynucleotide recycling in mitochondria, cause muscle- or liver-specific forms of MDS, respectively. Likewise, mutations in p53-ribonucleotide reductase subunit 2 (p53-R2) and thymidine phosphorylase (TP), two cytosolic enzymes controlling the *de novo* biosynthesis of deoxynucleotides (p53-R2), or the catabolism of nucleotide precursors (TP), are responsible for severe myopathic MDS with proximal tubule insufficiency (5), and myoneurogastrointestinal encephalomyopathy (MNGIE) (6), respectively. Also certain recessive mutations in the catalytic subunit of mtDNA-specific polymerase γ (7,8), and Twinkle, the mtDNA helicase (9,10), can cause different forms of

---

*To whom correspondence should be addressed at: Unit of Molecular Neurogenetics, IRCCS Foundation Neurological Institute 'C. Besta', Via Temolo 4, 20126 Milan, Italy. Tel: +39 0223942630; Fax: +39 0223942619; Email: zeviani@istituto-besta.it

hepatocerebral MDS. These proteins are all involved in the maintenance of mtDNA, either by controlling the supply of deoxynucleotides to, or by carrying out the synthesis of mtDNA. However, for other MDS-associated genes, the mechanism that links mutations to mtDNA depletion is unclear, and the very function of the corresponding proteins remains elusive. This uncertainty is well illustrated by *SUCLA2* and *SUCLG1*, encoding two isoforms of Krebs-cycle succinyl–CoA ligase, which are involved in encephalomyopathic MDS (11,12), and by *MPV17*, a gene on human chromosome 2 that we showed to be responsible for a peculiar form of hepatocerebral MDS (13). Additional *MPV17* mutant patients have later been reported in different ethnic backgrounds (14–16). The onset of the *MPV17*-associated disease is typically heralded by severe hypoglycemic crises in early infancy, associated with rapidly progressive deterioration of hepatic function, leading to liver cirrhosis and failure. Prevention of hypoglycemic episodes by frequent meals, based on prompt-release carbohydrates such as corn starch, can be effective in limiting hepatic damage (13). Nevertheless, in spite of the possibility to obtain partial control of fatal metabolic accidents, the surviving patients invariably progress in their liver degeneration, and develop neurological symptoms in their childhood. The full-blown syndrome has been thoroughly investigated in subjects affected by Navajo neurohepatopathy (NNH), a disease that has been known for decades to afflict the Navajo people of South-western USA. NNH was recently attributed to a specific mutation in the MPV17 protein, the p.R50Q, which originated from a single ancestral carrier common to all NNH patients (17). Clinical features of NNH/MPV17 syndrome include sensory motor neuropathy with ataxia, leukoencephalopathy, corneal ulcerations, acral mutilation, poor weight gain, short stature, sexual infantilism, serious systemic infections, and of course liver derangement (18). The same p.R50Q mutation responsible for NNH was previously found in a large *MPV17*-associated MDS family from Southern Italy (13), but the mutational event was proven to have occurred independently in the two family sets (19).

The *Mpv17* gene was first identified in laboratory mice created by random insertion of a retroviral construct in the genome of mouse embryonic stem cells (20). The *Mpv17*$^{-/-}$ mice showed severe kidney dysfunction dominated by proteinuria due to focal segmental glomerulosclerosis (FSGS) (21). The onset was in early mouse adulthood (2–3 months after birth) and the course was progressive, leading to systemic hypertension but no renal failure (22). In combination with the kidney phenotype, the *Mpv17*$^{-/-}$ mice displayed degeneration of the inner ear structures, particularly of the organ of Corti and *stria vascularis*, determining profound hearing loss (23,24). However, after a few generations the renal phenotype was no longer reported in *Mpv17*$^{-/-}$ mice, whereas the cochlear defect persisted.

In contrast with early reports, that assigned the Mpv17 protein to the peroxisomal compartment (25), we clearly demonstrated that this ubiquitously expressed, relatively small ($\sim$19.5 kDa) polypeptide is exclusively present in, and tightly anchored to, the inner membrane of mitochondria by four transmembrane domains (13). We also showed that in the *Mpv17*$^{-/-}$ mice as in the *MPV17* mutant patients, liver mtDNA content was profoundly reduced relative to Controls (13).

In spite of these discoveries, the very function of Mpv17 in mitochondrial biogenesis remains unknown, as well as the mechanism leading to tissue-specific mtDNA depletion in both mutant mice and men. To gain insight into this matter, we have further characterized the clinical features, course, and organ-specific physiopathology of the *Mpv17*$^{-/-}$ mouse model.

RESULTS

Clinical and morphological findings

Animal studies were approved by the animal welfare ethics committee of the 'Carlo Besta' Neurological Institute, in accordance with the Institutional Animal Care and Use Committee guidelines. Standard food and water were given *ad libitum* except for *ad hoc* experiments.

The *Mpv17*$^{-/-}$ mice did not develop overt hepatic failure at any age. Light microscopy examination showed neither massive necrosis nor cirrhosis in mice as old as 2 years, in contrast to what is observed in *MPV17* mutant infants. However, morphological alterations were present in the liver parenchyma starting from 5 months of age, consisting of swelling of hepatocytes with collapse of sinusoidal spaces, shrinking of nuclei in several cells, scattered degeneration of discrete areas of hepatic lobules, and inflammatory infiltrates concentrated in the portal triads (Fig. 1A). Neither accumulation of lipid droplets, nor fibrosis, nor proliferation of the bile ductular system was observed. Concomitant reduction in the cytochrome-c-oxidase (COX)-specific reaction was detected by histochemical staining (Fig. 1B). These lesions were progressive, starting from 5 months of age onward. AST, ALT and CK enzyme levels were constantly high in blood of $-/-$ mice (Supplementary Material, Table S1), ostensibly indicating subclinical hepatic and muscular damage. The blood lactate levels were moderately elevated as well, suggesting partial impairment of mitochondrial respiration (Supplementary Material, Table S1).

Although a Rotarod test failed to reveal significant impairment of motor skills (data not shown), in skeletal muscle sections of 1-year-old *Mpv17*$^{-/-}$ mice several fibers (5–6%) stained negative to the histochemical reaction to COX, indicating the presence of a subclinical mitochondrial myopathy (Fig. 1C). No alterations in muscle were present in 5-month-old *Mpv17*$^{-/-}$ mice (data not shown).

Electron microscopy examination was normal in hepatocytes of 15- and 60-day-old *Mpv17*$^{-/-}$ livers (data not shown), but mitochondrial ballooning and disappearance of the internal cristae was consistently observed in older *Mpv17*$^{-/-}$ mice, with proliferation of membranes surrounding the altered organelles (Fig. 1D). These abnormalities were not present in the mitochondria of other tissues (data not shown).

In infants, hypoglycemic episodes occur after 3–4 h of fasting. However, 48 h fasting failed to induce hypoglycemia in 2-month-old *Mpv17*$^{-/-}$ as well as *Mpv17*$^{+/+}$ mice (Supplementary Material, Fig. S1). An intra-peritoneal glucose tolerance test was normal in 2-month-old *Mpv17*$^{-/-}$ mice (Supplementary Material, Fig. S2). Prolonged exposure to low temperature is a stress condition that stimulates activation of heat production by mitochondrial respiration. We failed to
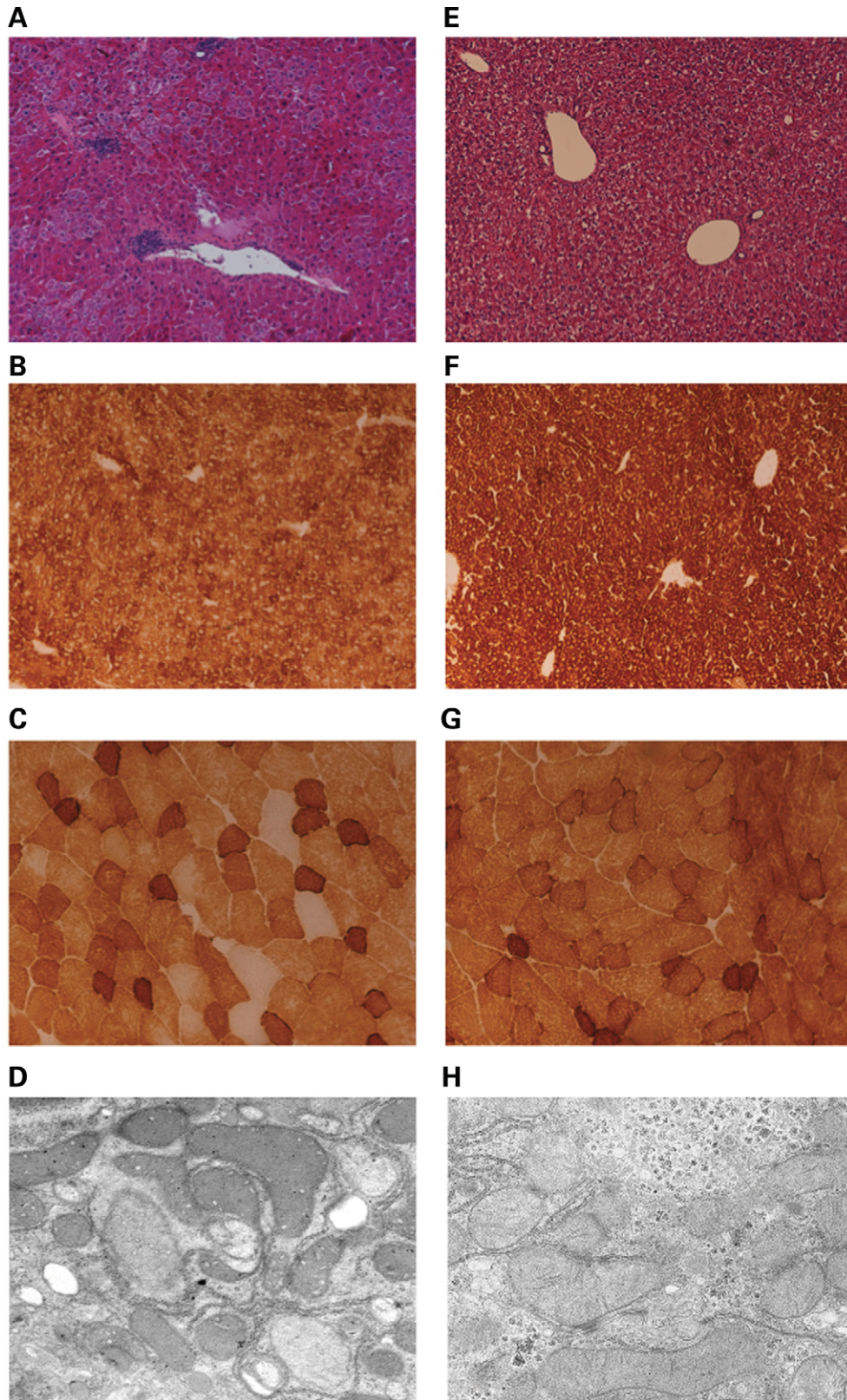
Figure 1. Histological and histochemical analysis. (**A**–**D**) Refer to $Mpv17^{-/-}$ mice; (**E**–**H**) refer to $Mpv17^{+/+}$ mice. (A and E) Liver H&E (×20): 2 years of age; (B and F) liver COX (×20): 1 year of age; (C and G) muscle COX (×20): 1 year of age; (D and H) electron microscopy ultrastructure of liver hepatocytes (×10 400): 1 year of age (see text for details).
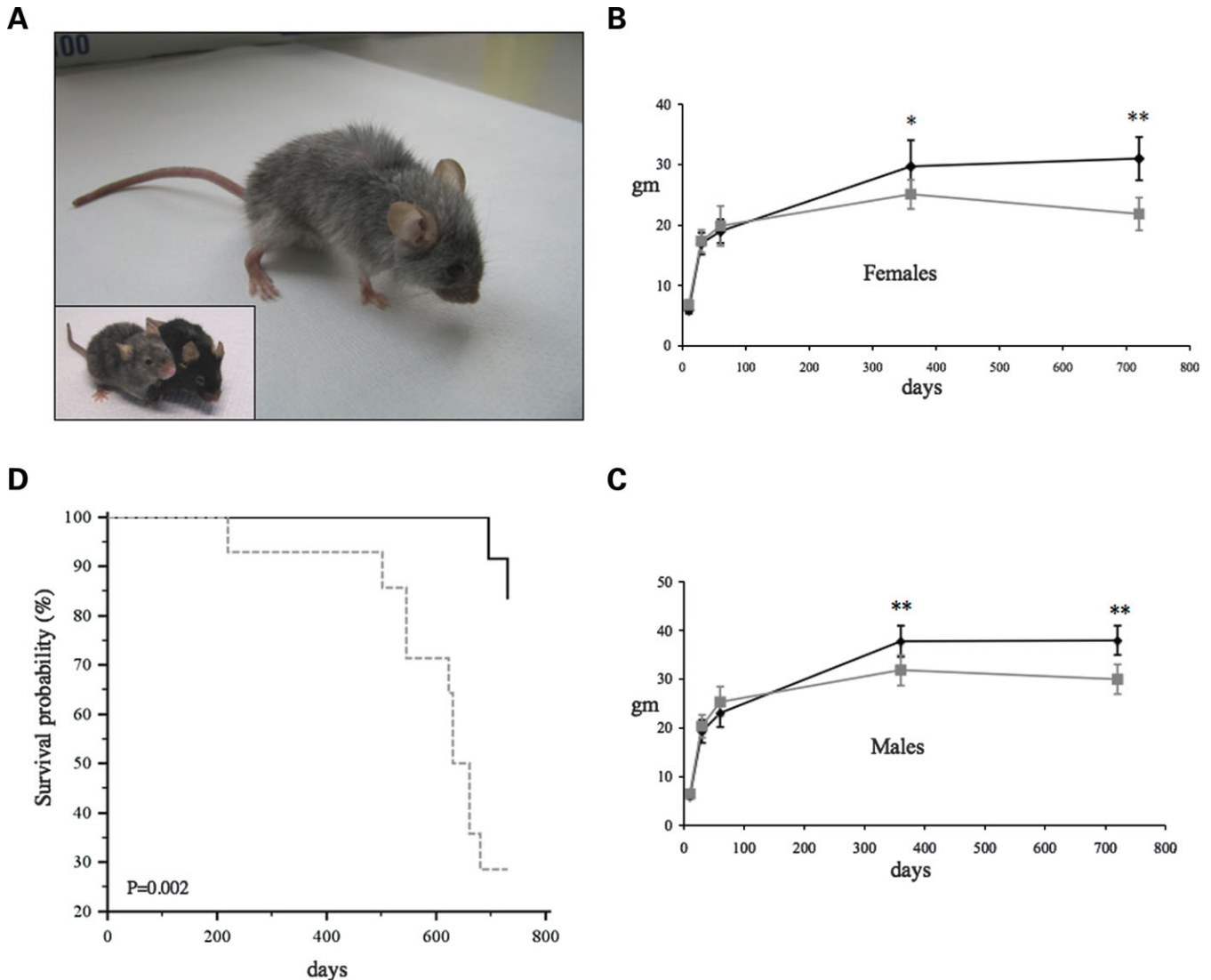
Figure 2. Clinical features. (**A**) A 2-year-old $Mpv17^{-/-}$ individual. The inset shows $-/-$ (gray) and $+/+$ (black) littermates at 1 year of age; (**B** and **C**) body weight at different ages in $-/-$ (gray line) and $+/+$ (black line) male and female individuals. A single asterisk indicates a Student's *t-test* $P = 0.01$; a double asterisk indicates $P = 0.002$; (**D**) Kaplan–Meier survival probability, $P = 0.002$ is the value of the log-rank test.

observe any clinical symptom referable to hypothermia in both 2-month-old $Mpv17^{-/-}$ and $Mpv17^{+/+}$ littermate mice maintained at $4°C$ for 72 h. Lastly, valproic acid is an anti-epileptic drug which is highly hepatotoxic, and may be fatal in some forms of hepatocerebral MDS, e.g. *POLG*-associated Alpers–Huttenlocher syndrome (8). Intra-peritoneal administration of 30 mg/kg valproate for 5 days failed to induce either morphological or biochemical abnormalities in the liver of $Mpv17^{-/-}$ mice.

Taken together, these results demonstrate a remarkable refractoriness of the $Mpv17^{-/-}$ mice to liver damage, in spite of the extremely reduced levels of mtDNA documented previously (13) and reconfirmed in this work (discussed later).

Clinical time course

Next, we asked whether the ablation of Mpv17 could produce age-dependent symptoms later in life, and affect lifespan. Two large series of $Mpv17^{-/-}$ and $Mpv17^{+/+}$ littermates were maintained under observation in standard captivity conditions for over 2 years.

We first observed that the coat of $Mpv17^{-/-}$ mice invariably turned gray 5–6 months after birth, while that of $+/+$ littermates remained uniformly black, as typical of the C57B/6 strain background of our mice (Fig. 2A). We then measured a significantly lower body weight of $Mpv17^{-/-}$ versus $Mpv17^{+/+}$ mice after 1 year of life for both males (Fig. 2B) and females (Fig. 2C). Finally, the survival probability (Fig. 2D) was highly significantly reduced in a group of $Mpv17^{-/-}$ mice (n. 14) versus a group of $+/+$ littermates (n. 12), both reared and kept in identical conditions (Kaplan–Meier log-rank test $P = 0.002$). The median lifespan (in days) of the $Mpv17^{-/-}$ group was 645 days. This result prompted us to re-evaluate morphological, biochemical and clinical features of our mice at late age.

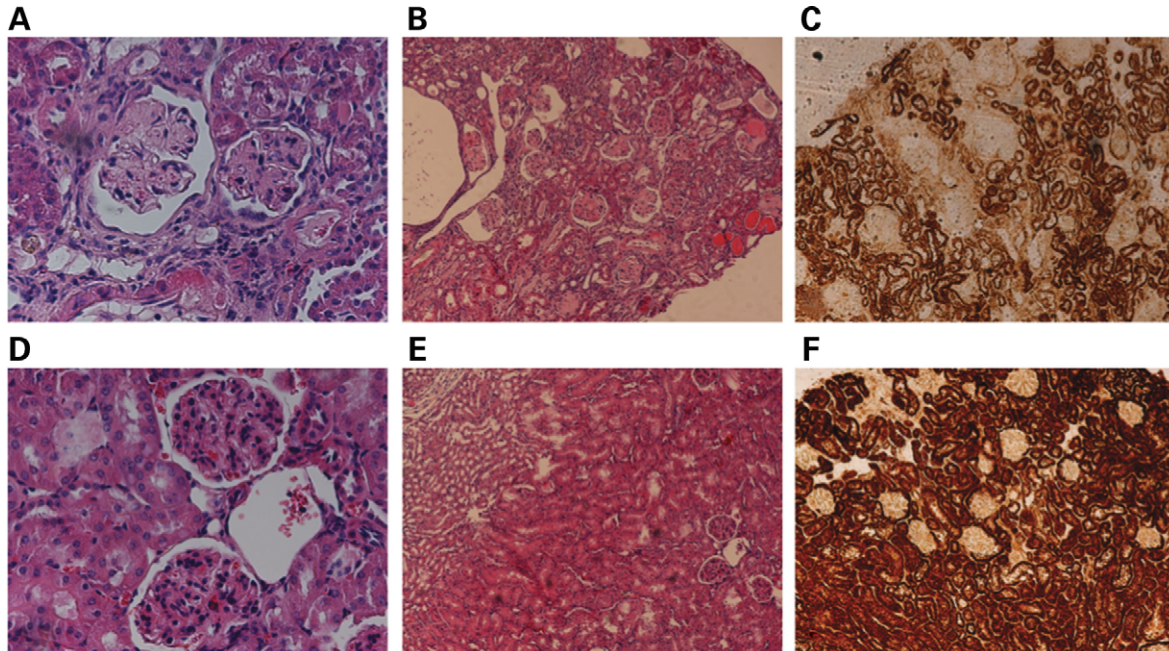When the kidney of 18-month-old $Mpv17^{-/-}$ mice was examined, we observed progressive FSGS, which at 2 years

Figure 3. Histology and histochemistry of kidney in 2-year-old mice. (**A**–**C**) Refer to $Mpv17^{-/-}$ mice; (**D**–**F**) refer to $+/+$ mice. (A and D) H&E ($\times 20$); (B and E) H&E ($\times 10$); (C and F) COX ($\times 10$) (see text for details).

of age evolved into frank degenerative changes of the glomeruli (Fig. 3A), accompanied by degenerative abnormalities in the tubular system, with dilation and formation of pseudocysts, parenchymal loss and interstitial fibrosis (Fig. 3B). Accordingly, $Mpv17^{-/-}$ mice showed the presence of massive proteinuria from 18 months of age onwards, but, surprisingly, creatinine and urea levels in blood remained within the normal range (Supplementary Material, Table S2) indicating that overt renal failure did not occur. Robust histoenzymatic reaction to COX was preserved in the epithelial cells of Bowman capsule, cortical tubules and medullary pyramids of $Mpv17^{-/-}$ kidneys at any age, although it appeared somewhat reduced in aged $Mpv17^{-/-}$ mice compared with $Mpv17^{+/+}$ individuals. As shown in Figure 3C, the COX reactivity was rather uneven in 2-year-old $Mpv17^{-/-}$ tubules, some of which stained normally, while others displayed reduced reactivity. In contrast, the cells of the glomerular tufts, which are mostly composed of endothelial cells, mesangial cells and podocytes, were much less reactive to COX in both groups of samples at any age; nevertheless, COX-specific staining of $Mpv17^{+/+}$ glomeruli was generally more intense than that of $Mpv17^{-/-}$ glomeruli, especially in 2-year-old mice (Fig. 3C).

Lastly, because of the early change in coat pigmentation and late-onset thinning of the skin, we also examined skin histology of 2-year-old $Mpv17^{-/-}$ versus $Mpv17^{+/+}$ mice. As shown in Figure 4A, the $Mpv17^{-/-}$ mice displayed severe atrophy of the skin layers, with thinning of the epidermis, loss of subcutaneous fat, and disorganization of the muscle layer. The hair follicles were also severely hypotrophic in $Mpv17^{-/-}$ skin samples with concomitant reduction in number and size of the sebaceous glands and other *annexa*.

Characterization of mtDNA depletion and biochemical phenotype

In an earlier report we showed that the amount of mtDNA in liver of 7-month-old $Mpv17^{-/-}$ mice was as low as 5% as that of $Mpv17^{+/+}$ littermates, it was 25% in muscle, and normal or slightly reduced down to 70% in brain and kidney.

In order to evaluate whether the mtDNA copy number is dependent on $Mpv17$ gene dosage, we measured mtDNA content in livers of $Mpv17^{-/+}$ heterozygous and $Mpv17^{+/+}$ homozygous littermates at 7 months of age. There was no statistically significant difference between the two groups (data not shown), indicating that $Mpv17$ is indeed associated with a strictly recessive trait.

In order to establish the time course of the depletion during extrauterine life, we measured the mtDNA copy number in liver, muscle and brain of $Mpv17^{-/-}$ and $Mpv17^{+/+}$ littermates at different ages. As shown in Figure 5, the mtDNA content of $Mpv17^{+/+}$ mice showed a concordant age-dependent variation in the three tissues, with a steady increase from birth levels during the first 60–90 days of life, and a progressive reduction afterwards. However, the mtDNA content remained constantly very low in liver and low in muscle of $Mpv17^{-/-}$ mice, while a variation similar to that of $Mpv17^{+/+}$ littermates was found in the $Mpv17^{-/-}$ brains. In liver, the mtDNA copy number per diploid nuclear genome, equivalent to one cell nucleus, was 1366 ± 384 molecules/nucleus in 2-month-old $Mpv17^{+/+}$ mice versus 93 ± 73 in $Mpv17^{-/-}$ littermates. In muscle of the same groups of mice the mtDNA copy number/nucleus was 3321 ± 835 in $Mpv17^{+/+}$ versus 611 ± 191 in $Mpv17^{-/-}$ samples.

In order to see whether the mtDNA abnormalities observed in tissues could also be reproduced in a cell culture system,
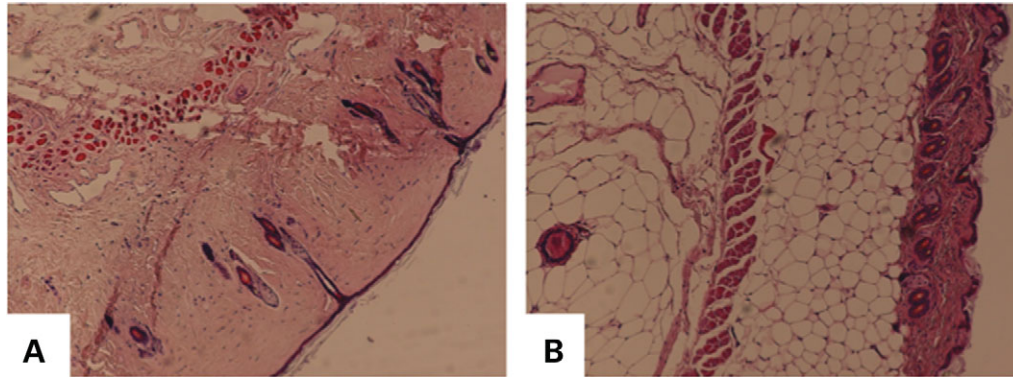
Figure 4. Histology of 2-year-old skin. H&E ($\times$10). (**A** and **B**) Refer to $Mpv17^{-/-}$ and $Mpv17^{+/+}$ mice respectively (see text for details).
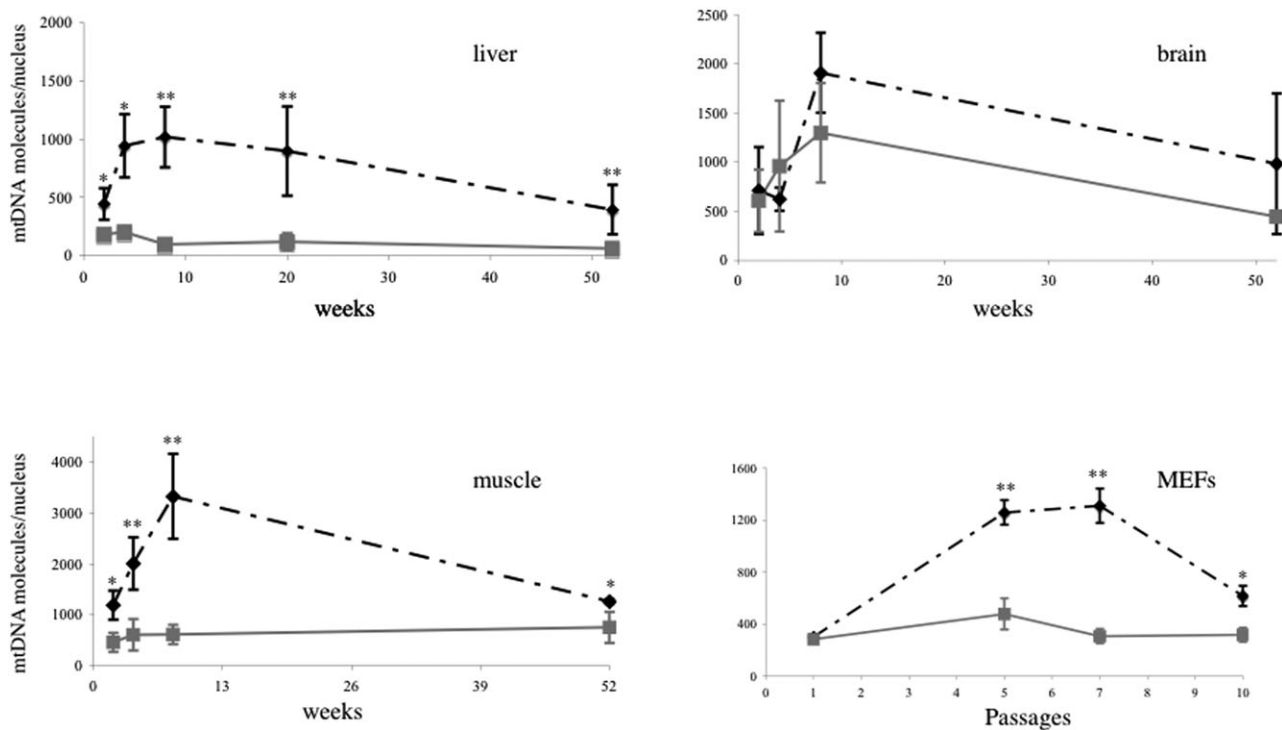

Figure 5. Real-time PCR analysis of mtDNA copy number from 2 weeks to 1 year of age. The gray line refers to $Mpv17^{-/-}$ mice; the black line refers to $Mpv17^{+/+}$ littermates. A single asterisk indicates a Student's *t*-test $P \leq 0.01$; a double asterisk indicates $P \leq 0.002$.

we characterized $Mpv17^{-/-}$ and $Mpv17^{+/+}$ mouse embryonic fibroblasts (MEFs) at different passages. We found that in $Mpv17^{+/+}$ MEFs, as in $Mpv17^{+/+}$ tissues, the mtDNA content increased over time, whereas it progressively declined in $Mpv17^{-/-}$ MEFs from passage 1 to 10 (Fig. 5). As a consequence, the relative mtDNA content, which was similar in $Mpv17^{-/-}$ versus $Mpv17^{+/+}$ cell lines at the first passage (P1), decreased by 60–80% at P5 and remained low in later passages (Fig. 6A).

Marked reduction in mtDNA was also observed in confluent (non-proliferating) MEFs, cultured in the absence of fetal calf serum (serum deprivation) (Fig. 6B). These data indicate that mtDNA depletion can occur in MEFs by inducing aging or stress conditions that require an efficient OXPHOS (oxidative phosphorylation) system.

Because of the late renal phenotype manifested by >-18-month-old $Mpv17^{-/-}$ mice, we measured the mtDNA content in the renal parenchyma 1-year and 2-year-old mice. The amount of mtDNA was virtually identical in whole kidneys of three $Mpv17^{+/+}$ versus three $Mpv17^{-/-}$ mice at 1 year of age. In particular, the mtDNA copy number was 728 ± 52 mtDNA/nucleus in $Mpv17^{+/+}$ and 696 ± 60 mtDNA/nucleus in $Mpv17^{-/-}$ samples. However, the mtDNA content was reduced to $\sim$47% in the $Mpv17^{-/-}$ versus $Mpv17^{+/+}$ 2-year-old groups, each consisting of three mice. In particular, the mtDNA copy number per cell was 1012 ± 156 mtDNA/nucleus in $Mpv17^{+/+}$ versus 470 ± 170 mtDNA/nucleus in $Mpv17^{-/-}$ samples (Student's *t*-test $P = 0.015$).

Since the predominant kidney abnormality consisted of severe proteinuria, i.e. an alteration of the glomerular filtering
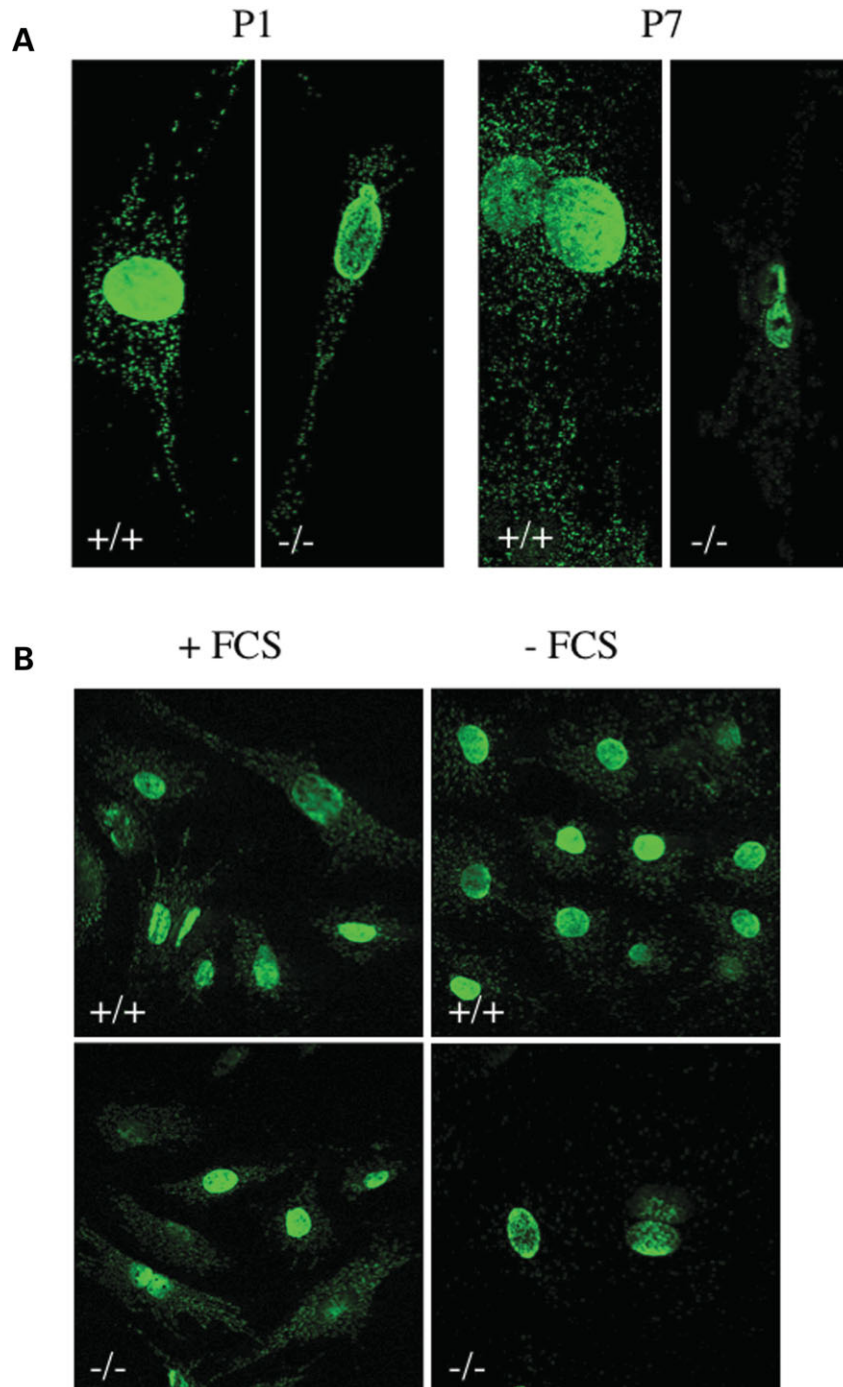
Figure 6. Immunofluorescence studies on MEF cultures. The green fluorescence refers to nuclear and mitochondrial DNA visualized with an anti-DNA antibody. (**A**) MEF cultures at passage 1 (P1) and passage 7 (P7); (**B**) MEF cultures with (+FCS) or without (−FCS) 10% fetal calf serum (see text for details).

proficiency, we also measured the mtDNA content in pools of glomeruli and cortical tubules microdissected from kidneys of two 6-month-old and two 2-year-old littermates (Table 1). The mtDNA molecules/diploid nucleus was significantly less in $Mpv17^{-/-}$ versus $Mpv17^{+/+}$ glomeruli ($P < 0.025$), but the difference was much higher in 2-year-old mice ($P < 0.00007$). Contrariwise, no significant differences were observed in $Mpv17^{-/-}$ tubules versus $Mpv17^{+/+}$ tubules at 6 months ($P = 0.66$) and 2 years. ($P = 0.56$).

Transcriptional regulation

The biochemical activities of respiratory chain complexes I and IV declined rapidly after birth, and remained stably low, in $Mpv17^{-/-}$ liver homogenates, to ∼30–40% of those measured in $Mpv17^{+/+}$ littermates (Table 2). No significant differences were detected for the same activities measured in other tissues of the two groups of mice, including muscle, brain and kidney. Therefore, the impairment of mtDNA-related respiratory chain

Table 1. mtDNA copy number in tubules and glomeruli of $Mpv17^{+/+}$ and $Mpv17^{-/-}$ mice at 6 months and 2 years of age

	6 months Tubules	Glomeruli	2 years Tubules	Glomeruli
+/+	454 + 49	203 + 24	1244 + 444	463 + 155
−/−	574 + 115	156 + 29*	1059 + 298	151 + 59**

*$P < 0.025$ (Student's *t-test*); **$P < 0.00007$.

Table 2. Biochemical activities of complexes I and IV in liver homogenate (each group was composed of 4–6 individuals)

Weeks	Complex I/CS +/+	−/−	Complex IV/CS +/+	−/−
2	107.9 + 7.4	126.5 + 21.2	120.7 + 15.0	107.9 + 17.4
4	44.7 + 1.7	28.6 + 4.3**	86.1 + 13.1	69.0 + 13.9*
8	45.6 + 11.4	18.7 + 2.8**	76.6 + 11.8	30.0 + 11.6**
52	52.3 + 15.4	23.4 + 3.4**	80.65 + 15.3	19.7 + 3.4**

Values are expressed as ratio between specific activities expressed as (nmol/min/mg non-collagen protein); CS, citrate synthase.
*$P < 0.05$ (Student's *t-test*); **$P < 0.008$.

activities was disproportionately mild when compared with the profound decrease in the mtDNA copy number detected in $Mpv17^{-/-}$ liver, as well as $Mpv17^{-/-}$ muscle, tissues.

In order to evaluate whether compensatory mechanisms were active in mtDNA-depleted tissues, we first measured steady-state transcription and translation of mtDNA genes in the liver of −/− and +/+ mice at different ages. Figure 7A shows that the mtDNA-specific RNA levels, visualized by northern blotting, were only moderately reduced in $Mpv17^{-/-}$ mice compared with the $Mpv17^{+/+}$ littermates at all examined ages. An even less significant decrease was found in some of the corresponding proteins, for instance COX1, visualized by western blotting (Fig. 7B).

These results suggested the existence of a compensatory mechanism at the level of mtDNA transcription and possibly translation as well. To test this hypothesis, we carried out pulse-chase *in organello* transcription experiments in isolated mitochondria of 6-month-old $Mpv17^{-/-}$ versus $Mpv17^{+/+}$ mice. Transcription was analyzed after 2, 4, 5 and 6 h of incubation. As shown in Figure 7C, the amount of mtDNA-specific transcripts in $Mpv17^{-/-}$ mice was lower than in $Mpv17^{+/+}$ littermates in absolute terms, but the efficiency of transcription was much higher, considering that the content of mtDNA was extremely reduced, in fact virtually undetectable. 1n both $Mpv17^{-/-}$ and $Mpv17^{+/+}$ samples the *de novo* transcription increased up to the fifth hour, to then decrease at the sixth. Taken together, these results indicate the existence of vigorous transcriptional compensation of mtDNA depletion in $Mpv17^{-/-}$ liver.

We next investigated whether this compensatory effect could be due to differential expression of factors involved in mitochondrial biogenesis, mtDNA maintenance or mtDNA transcription. To this aim, we analyzed by real-time PCR the expression levels of a host of suitable genes in $Mpv17^{-/-}$ versus $Mpv17^{+/+}$ 6-month-old livers. As shown in Figure 8A, the analysis included factors activating mitochondrial biogenesis, such as

Pgc1α, Pgc1β and Nrf1 (26,27), and factors involved in mtDNA replication (Pol γA, Twinkle) and/or transcription (Tfam, TfbIM, TfbIIM, Mterf1, Polrmt) (28). The only transcript that was expressed differently in the two groups of mice was Mterf1, which was consistently and significantly reduced by ∼40% in $Mpv17^{-/-}$ liver samples. Interestingly, identical or similar results were obtained for Mterf1 in muscle but not in brain of $Mpv17^{-/-}$ mice, in agreement with the amount of mtDNA measured in the same tissues (Fig. 8B).

The reduction in Mterf1 transcript was accompanied by reduced amount of the corresponding protein in liver mitochondria (∼60–70%), as shown by western blot analysis using an anti-Mterf1 polyclonal antibody (Fig. 8C). In order to evaluate whether reduced expression of Mterf1 was sufficient to determine a change in the ratio between ribosomal and protein-encoding mtDNA transcripts, we measured the band intensity of the *in organello* transcribed cytochrome c oxidase subunit I (COI) and 16S rRNA species shown in Figure 7C at 2 and 4 h. The COI/16S rRNA ratio at the second hour was 2.05 in the $Mpv17^{-/-}$ versus 1.49 in the $Mpv17^{+/+}$ liver mitochondria; at the fourth hour it was 2.43 versus 1.09.

DISCUSSION

The $Mpv17^{-/-}$ mice are the first example of an animal model of MDS. TK2 knockout (29) and knockin (30) mice have more recently been reported.

We showed that in young mice, as in humans, the ablation of $Mpv17$ determines a profound reduction in mtDNA content in liver and, to a lesser extent, in skeletal muscle, but neither in brain nor in kidney. Measurement at different ages revealed that, in keeping with previous data in $Mpv17^{+/+}$ mice the mtDNA content varied over time in liver and muscle (31), while it remained constantly low throughout life in the same tissues of $Mpv17^{-/-}$ mice. This was not the case for $Mpv17^{-/-}$ brain tissue, in which both the absolute mtDNA content and its age-dependent variation were similar to those of $Mpv17^{+/+}$ brains. Although the mechanistic role of Mpv17 remains elusive, these results demonstrate that the absence of this protein impairs a dynamic control on mtDNA copy number, in a tissue-specific and possibly developmentally regulated manner. This conclusion is also supported by studies in cell cultures, since MEFs from $Mpv17^{-/-}$ mice failed to show any mtDNA depletion at the beginning, but did develop it after several passages, a situation that simulates an aging process, or after serum deprivation, a paradigm of cellular stress.

The low mtDNA content in liver was associated with surprisingly mild morphological alterations of its cytoarchitecture, whereas, at the ultrastructural level, mitochondria of $Mpv17^{-/-}$ hepatocytes were profoundly altered, especially in 5-month and older mice. Mitochondria became ballooned, the cristae disappeared, an electron-dense amorphous material accumulated in the matrix, and the organelles were surrounded by membranous structures, probably derived from a proliferation of endoplasmic reticulum. Although similar ultrastructural changes were also described in *MPV17* mutant patients (14), they are not specific to this condition, having been reported in other forms of hepatocerebral MDS (32).
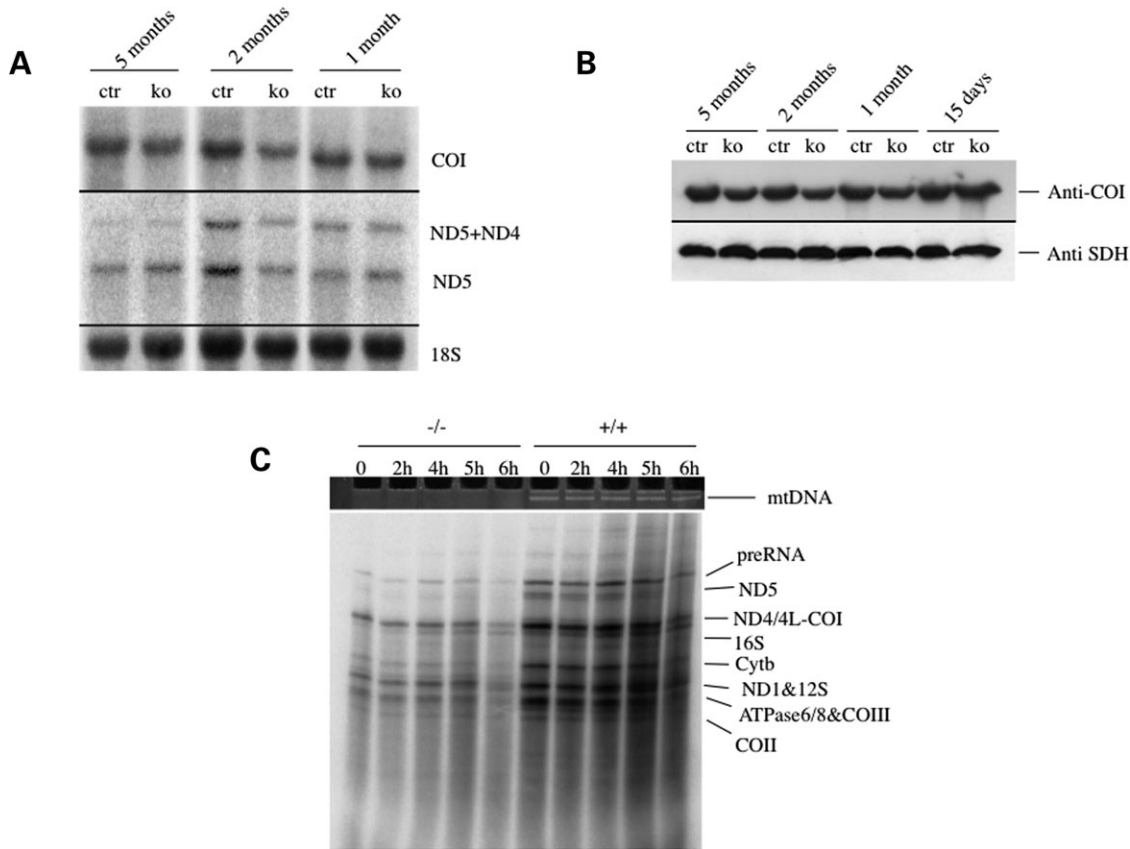
Figure 7. RNA and protein blot analyses of $Mpv17^{-/-}$ and $Mpv17^{+/+}$ littermates at different ages. (**A**) Northern blot analysis of mtDNA transcripts. The nuclear multicopy gene encoding 18S ribosomal RNA was used for standardization, preND5 refers to the ND5 + ND4 pre-mRNA; (**B**) protein blot analysis using an antibody specific to COX1 subunit. An antibody against the 30 kDa subunit of SDH was used for standardization; (**C**) pulse-chase *in organello* mitochondrial RNA synthesis. Notice the reduction in band intensity at 6 h in both $-/-$ and $+/+$ samples. The ethidium-bromide staining of the mtDNA-specific band is shown on top: in contrast with the $+/+$ samples, the $-/-$ samples have hardly any detectable mtDNA.

In addition, no such changes were found in extrahepatic tissues of our mice, which were also lacking Mpv17 but have normal or moderately reduced amount of mtDNA. Taken together, these results suggest that the mitochondrial abnormalities seen in $Mpv17^{-/-}$ liver are secondary to functional impairment of the organelles, rather than reflecting a role of Mpv17 in controlling the shape of the cristae and the structure of the inner mitochondrial compartment.

The very low content of mtDNA in liver was associated with milder decrease in mtDNA-related respiratory chain activities, including those of complexes I and IV. Incidentally, the activity of an mtDNA-independent respiratory chain complex such as succinate dehydrogenase (SDH) was also found normal in a previous study on 6-month-old $Mpv17^{-/-}$ livers (13), as was the SDH histochemistry in the same tissue (data not shown). These data explain the overall preservation of functional liver proficiency and the lack of the dramatic morphological changes that were documented in human patients. In contrast with the human condition, the absence of $Mpv17$ was not associated with metabolic fragility of the $Mpv17^{-/-}$ mice, which failed to develop fasting-induced hypoglycemia, increased sensitivity to hepatotoxic valproate, or hypothermia by prolonged exposure to cold. Based on analysis of transcription and translation of mtDNA in liver mitochondria, we demonstrated a remarkable

compensatory mechanism that maintains cellular respiration of $Mpv17^{-/-}$ mouse liver (and muscle as well) at levels compatible with virtually normal life in captivity. In particular, both northern blotting and *in organello* transcription analyses showed that one compensatory key point is at the level of transcription, since the ratio between mtDNA transcripts and mtDNA content in $Mpv17^{-/-}$ organelles was several fold higher than in $Mpv17^{+/+}$ organelles. As a result, the amount of mtDNA-specific translation products was comparable in livers of $-/-$ versus $+/+$ mice.

Functional compensation was recently reported in several mtDNA-depleted tissues of $Tk2^{-/-}$ mice (30), and transcriptional compensation was demonstrated in heterozygous *Tfam* knockout mice (33), and in skeletal muscle of patients with *TK2* mutations (34). Thus, compensation at the transcriptional or translational level may well be a general phenomenon in response to mtDNA depletion.

These results prompted us to evaluate the expression level of several factors involved in mtDNA transcription/maintenance. A 40% reduction was consistently found in the steady-state transcript level of Mterf1 in liver, while all other genes examined were not differentially expressed between $+/+$ and $-/-$ mice. A concordant reduction in Mterf1 protein was immunodetected using a specific antibody. Mterf1 is a transcriptional termination factor that blocks the
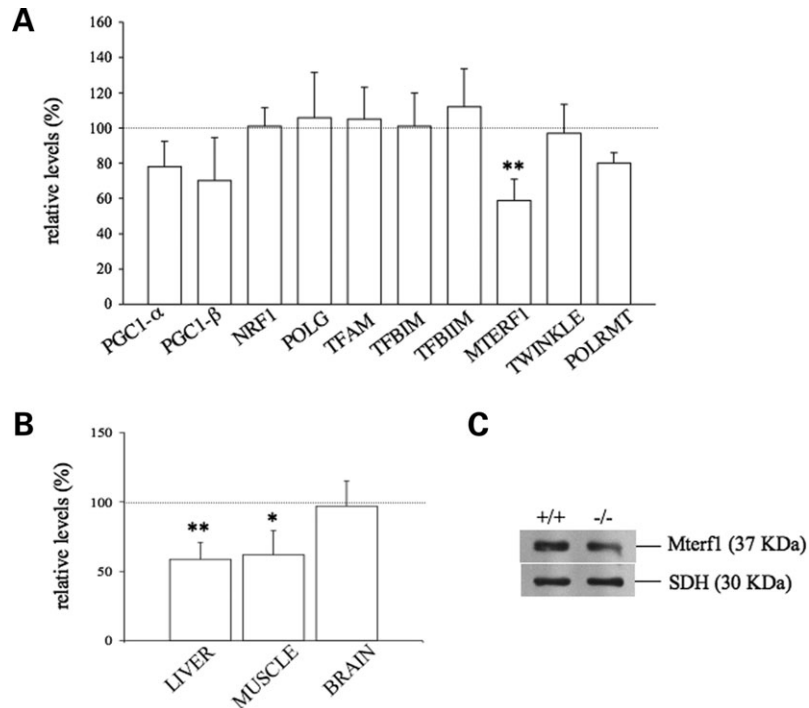
Figure 8. Real-time PCR quantification of mRNA transcripts from genes involved in mtDNA biogenesis. (**A**) Liver transcripts of 2-month-old $-/-$ mice. PGC1-α and PGC1-β, peroxisome proliferative activated receptor gamma coactivator 1, isoforms α and β; NRF1, nuclear respiratory factor 1; POLG, polymerase γ subunit A; TFAM, transcription factor A mitochondrial; TFBIM and TFBIIM, transcription factors BI and BII mitochondrial; MTERF1, mitochondrial termination factor 1; Twinkle, mitochondrial helicase; POLRMT, RNA polymerase mitochondrial; (**B**) Mterf1 transcript levels in different tissues of 2-month-old $Mpv17^{-/-}$ mice. The dotted lines indicate the mean levels obtained in Control littermates, taken as 100%; (**C**) Mterf1 western blot analysis. The SDH-specific band was used as a standard for protein content.

heavy-strand mtDNA polycistronic transcription by looping mtDNA across two binding sites: the heavy-strand promoter 2, HSP2, and a termination site within the tRNA$^{Leu(UUR)}$ gene, adjacent to the gene encoding 16S rRNA (35). As a consequence, Mterf1 decreases the HSP2-dependent expression of the mtDNA structural genes (and of many tRNA genes as well), which are all located downstream from the 16S rRNA gene, whereas transcription of the 12S and 16S rRNA genes, which can proceed from both HSP2 and from a second heavy strand promoter, HSP1, remains unaffected. As a result, the amount of rRNAs is 15–60-fold higher relative to mRNA (36,37). Thus, one of the physiological roles attributed to Mterf1 is to maintain mitochondrial 12S and 16S rRNA transcript levels in excess relative to mRNA transcripts, so as to prevent that the endowment in ribosomes of mitochondria becomes a limiting factor to protein translation. The increase *in organello* transcription of COI mRNA relative to 16S rRNA that we observed in $Mpv17^{-/-}$ liver mitochondria does indeed support this hypothesis. Likewise, the observation that Mterf1 transcript was also reduced in $Mpv17^{-/-}$ muscle, another tissue with significant mtDNA depletion, whereas it was normal in $Mpv17^{-/-}$ brain, which had virtually no or very little mtDNA depletion, suggests that this variation is functionally relevant. Taken together, our data suggest for Mterf1 a role in the transcriptional (and translational) compensatory response to reduced mtDNA copy number in specific $Mpv17^{-/-}$ organs. Interestingly, a general increase in transcription of mitochondrial RNAs is associated with ablation

of mouse Mterf3, which is part of the same Mterf protein family that includes Mterf1 (38).

Some of the clinical features of the $Mpv17^{-/-}$ mouse were not observed in the human equivalent, possibly because their onset appeared late in mouse life, while human *MPV17*-MDS is an early-onset disorder, which usually leads patients to death in infancy or childhood.

For instance, $Mpv17^{-/-}$ mice showed a progressive loss of the coat color, starting several months after birth. Hair graying is not related to normal aging in the mouse, as also demonstrated by our own observation that Control littermate mice remained uniformly black well after 2 years of age. The knockout mouse for Bcl2, a mitochondrial anti-apoptotic factor, turns gray because of loss of the melanocyte precursor stem cells in the hair follicle niche (39,40). Given the mitochondrial localization of Mpv17, a pro-apoptotic mechanism could also be acting in the $Mpv17^{-/-}$ model. For instance, reactive oxygen species (ROS) can damage melanocytes either directly or by inducing mitochondrial apoptosis (41), and increased production of ROS was previously reported in fibroblasts of $Mpv17^{-/-}$ mice (25,42). In addition, the skin of aged $-/-$ individuals showed severe atrophy, particularly affecting the subcutaneous fat and muscular layer. These features can be the result of the compromised clinical conditions of these mice; however, they could also reflect a more specific pathogenic process, since similar findings were recently reported in Tk2 knockout mice (29), another model of mtDNA depletion.

The most striking organ pathology of $Mpv17^{-/-}$ mice consisted of FSGS, followed by hyaline degeneration and loss, degenerative changes of the tubular system, and fibrosis. As a consequence, the $Mpv17^{-/-}$ mice developed massive proteinuria, due to abnormal leakiness of the glomerular filtering system. Most likely as a consequence of the kidney disease, they showed progressive downhill of their health conditions starting from 18 months after birth, with highly significant reduction in average and maximum lifespan, compared with the $+/+$ littermates.

The occurrence of FSGS, associated with extensive flattening of the foot processes of podocytes, was reported in the first papers on the $Mpv17^{-/-}$ mouse model (20,42). The ultrastructural alterations occurred after the maturation of podocytes, i.e. were not due to arrest in the full development of arborized foot processes that takes place after birth (21). The morphological alterations were associated with proteinuria starting in mouse early adulthood ($\sim$50 days after birth). However, the kidney phenotype was no longer detected after a few generations, at least within the lifetime considered by the examiners. We ourselves failed to find any trace of proteinuria or renal pathology in $Mpv17^{-/-}$ mice as long as 12 months after birth (13). Our present data show that glomerular damage still occurs in $Mpv17^{-/-}$ mice but starts much later in life. The reason for such a remarkable age-dependent timeshift of disease onset is unknown, but it could depend on a modification of the genetic background of the mice. For instance, the mouse strain of our own colony, C57/B6, is different from the mixed background (CFW) of the $Mpv17^{-/-}$ mice reported in the first papers.

Concomitant lesions of the membranous and cellular structures of the cochlear receptor were also reported in $Mpv17^{-/-}$ mice (23). Although in the present study we did not examine the inner ear, recent publications by others have confirmed the presence of severe cochlear lesions in the very same mouse colony used for our work (24).

The development of severe, progressive lesions in the renal glomeruli is indeed a remarkable finding, considering that in the bulk of kidney parenchyma we found hardly any mtDNA depletion in young mice, and moderate reduction in aged individuals, not in the least comparable with that found in the liver. In order to further investigate the molecular basis of this apparent discrepancy, we quantified the mtDNA content of cells in the glomerular tufts versus tubular epithelial cells. Glomeruli isolated by laser-microdissection from proteinuric $Mpv17^{-/-}$ kidneys displayed marked reduction in mtDNA content compared with those obtained from non-proteinuric $+/+$ kidneys of the same age, i.e. 2 years old. More than the absolute amount of mtDNA, we observed the same phenomenon in glomeruli as that found in liver, muscle, and MEFs, that is, the failure of $Mpv17^{-/-}$ cells to undergo the physiological increase (and variations) in mtDNA copy number detected in $Mpv17^{+/+}$ organs during post-natal lifetime. In addition, a significant trend toward reduction in glomerular mtDNA content was already detected in non-proteinuric, 6-month-old $Mpv17^{-/-}$ mice, implicating that proteinuria is the result of a chronic pathogenic process ultimately damaging glomerular structure and function. In contrast, no difference in mtDNA content was detected in the renal tubules of both young and old kidneys, consistent with the absence of tubular insufficiency in $Mpv17^{-/-}$ mice at any age.

Taken together, these results suggest that glomerular podocytes are exquisitely prone to marked mtDNA depletion, which become clinically relevant in aged $Mpv17$-less mouse kidneys. Although the mtDNA content of normal podocytes is already low, being associated with hardly any COX-specific histochemical reactivity (43), further reduction in mtDNA amount is likely to have functional consequences.

Glomerular filtering *per se* is an essentially passive phenomenon, but it requires the formation and maintenance of an intact and highly selective glomerular basement membrane (GBM). Anatomical and functional features of GBM are the results of interaction between endothelial cells of glomerular capillaries with podocytes. The latter are highly differentiated post-mitotic cells that maintain various energy-demanding functions including the synthesis and organization of cytoskeletal and extracellular matrix proteins. Earlier reports suggested that podocyte lesions of $Mpv17^{-/-}$ mice were associated with increased ROS production (25,42), and administration of ROS scavengers was also effective in preventing, or ameliorating, the proteinuria and focal nephrosclerosis in these mice (42).

FSGS is a major renal complication of mitochondrial cytopathies in humans (43), including mtDNA mutations such as the 3243A>G 'MELAS' transition in tRNA$^{\text{Leu(UUR)}}$, and single, large-scale mtDNA deletions (see reference 44 for a review on this issue). Mutant mice carrying a large deletion of mtDNA develop FSGS lesions, leading to death within 6 months due to renal failure (45). Rrm2b-knockout mice, equivalent to p53-R2 mutant patients, suffer both mtDNA depletion and glomerular hyaline degeneration with proteinuria (46). Finally, puromycin aminoglucoside nephrosis (PAN) is the best-described animal model of glomerular disease, evolving into FSGS. Kidney of PAN rats show reduction in respiratory chain enzymatic activities and oxygen consumption, with swelling of renal tubular mitochondria (43). PAN has been associated with decrease in mtDNA content to as low as 34% in rat kidney glomeruli at the FSGS stage (43). Early reports on $Mpv17^{-/-}$ mice have indeed shown that these mice were exquisitely sensitive to PAN (42). Again, PAN-induced proteinuria and glomerular lesions can be attenuated by exposure to antioxidants, suggesting that excessive ROS production is a pathogenic mechanism also in this condition (42).

In the light of the earlier considerations and of our own results, an excess of ROS could well occur as a consequence of OXPHOS failure in $Mpv17^{-/-}$ glomeruli, leading to podocyte damage and degeneration. These effects could in turn compromise the anatomical and functional integrity of the GBM, and determine both the proteinuria and the progressive morphological changes seen in the kidney of old $-/-$ individuals.

Neither the renal nor the inner ear pathologies were reported in *MPV17* mutant patients, including those affected by NNH. These symptoms are in fact reminiscent of a group of human genetic diseases characterized by the association of steroid-resistant proteinuric nephrosclerosis and perceptive hearing loss, known as Alport syndrome (OMIM #301050). Alport syndrome is caused by mutations in COL4A3, COL4A4 or COL4A5 genes, which encode the alpha-3,

alpha-4 and alpha-5 chains of type IV collagen. These cysteine-rich isoforms of type IV collagen are essential components of mature GBM. As a consequence, the GBM of Alport syndrome patients retains a fetal distribution of the cysteine-poor alpha-1 and alpha-2 isoforms of type IV collagen, which confer GBM a higher susceptibility to proteolytic attack by collagenases and cathepsins (47).

The renal and inner-ear damages are often accompanied by lesions in other organs, notably the epidermis and the eye. The latter include lesions of the retina (retinal flecks), lens (lenticonus and spherophakia) and cornea (posterior corneal dystrophy and recurrent corneal erosion). Interestingly, corneal ulcerations and corneal scarring are late manifestations of NNH that are allegedly attributed to, but not convincingly proven to derive from, anesthesia due to sensory peripheral neuropathy.

A mechanism similar to that acting in Alport syndrome has been hypothesized also in the pathogenesis of *Mpv17*-associated FSGS, since the lack of this protein in $-/-$ mice induces the overexpression of MMP-2, a metalloproteinase of the extracellular matrix present in both kidney and inner ear (48).

Although Alport syndrome has never been connected to mitochondrial dysfunction, other genetic disorders of collagen have been. For instance, missense mutations of COL6A, encoding the collagen-6 protein isoform, are responsible for relatively benign Bethlem myopathy (OMIM #158810), while non-sense mutations in the same gene cause the much more severe Ullrich myopathy (OMIM #254090). In mitochondria of both human patients and a COL6A-gene knockout mouse, malfunctioning or absence of collagen-6 is associated with a mitochondrial defect linked to dysregulation of the mitochondrial permeability transition pore (PTP) (49). This defect is corrected by cyclosporine A, an inhibitor of PTP opening (50,51).

Other human conditions resembling Alport syndrome are Epstein (OMIM #153650) and Fechtner (OMIM #153640) syndromes. These entities are variants of the same genetic defect, that is, mutations in the myosin heavy chain-9 non-muscle isoform (52). This protein has recently been shown to have a double localization: in the cytoskeletal framework, for instance in the stereocilia of the cochlear hair cells, as well as in the inner compartment of mitochondria (53).

Taken together, these considerations foster the interesting hypothesis that besides a role in controlling mtDNA copy number and ROS production, Mpv17 may be functionally linked to components of the extracellular matrix or of the cytoskeleton, which are involved in the integrity of the GBM and possibly other epithelial basement membranes in vertebrates, notably mammals.

MATERIALS AND METHODS

Genotyping

Diagnosis of the recombinant and wild-type alleles of the *Mpv17* gene was performed by PCR-based length polymorphism analysis on tail genomic DNA using suitable primers (Supplementary Material, Table S3). The recombinant allele corresponds to a PCR band of 234 bp, whereas the wild-type allele corresponds to a PCR band of 217 bp. The two bands were separated electrophoretically through a 2% agarose gel in TE and visualized under a UV screen.

Morphological analysis

For standard histology, 10 μm sections from different tissues were post-fixed in 4% paraformaldehyde; for histochemistry, samples were frozen in liquid-nitrogen cooled isopentane and 10 μm cryostat sections were used to visualize COX reactivity (54). For standard ultrastructural studies, fixation was by 2% glutaraldehyde in PBS.

Real-time PCR

Total DNA was extracted from tissues following standard procedures. For mtDNA content analysis, SYBR-GREEN real-time PCR was performed using primers specific to a mouse mtDNA fragment of the COI gene, and primers specific to RNaseP, a single copy gene taken as a nuclear gene reference (Supplementary Material, Table S4). Relative copy number was calculated from threshold cycle value (DCt), and the mtDNA copy number/cell was calculated as 2×2^{-DCt} to account for the two copies of RNaseP in each nucleus (55). Real-time quantitative PCR was carried out using an ABI PRISM 7000 Sequence Detection System. The amplification profile was according to a two-step protocol: one cycle at 50°C for 2 min, one cycle at 95°C for 10 min, and then 40 cycles of 95°C for 15 s and 60°C for 1 min. A final dissociation step (95°C for 15 s, 60°C for 20 s, 95° for 15 s) was added to assess for unspecific primer–dimer amplifications.

For the analysis of transcripts, total RNA was extracted from liquid-nitrogen snap-frozen liver and muscle specimens by Trizol, according to manufacturer instructions (Invitrogen, Carlsbad, CA, USA). Two microgram of total RNA was treated with RNase-free DNase and retro-transcribed by using the 'cDNA cycle' kit (Invitrogen). Approximately 2–5 ng of cDNA was used for real-time PCR assay using primers specific for amplification of several genes, according to the ABI-Primer Express software (Supplementary Material, Table S3). In some experiments, we microdissected discrete areas of 10 μm H&E stained cryostat sections under a laser-equipped Nikon Eclipse TE2000-S. Total DNA was extracted using the Microlysis™ kit (Microzone Limited, UK).

Northern blot

Total RNA was extracted from liver and muscle samples, as described, run on a formaldehyde agarose gel, and capillary blotted onto a nylon membrane (*N*+, Amersham) according to manufacturer instructions. Hybridization was carried out according to standard procedures, using probes specific for mouse COI, ND5, 18S, obtained by PCR amplification with suitable primers (Supplementary Material, Table S5).

In organello RNA synthesis

Mouse liver mitochondria were isolated as described (56), and *in organello* experiments were carried out as described (57). Briefly, mitochondria from one liver were suspended in

0.6 ml of incubation buffer (25 mM sucrose, 75 mM sorbitol, 100 mM KCl, 10 mM K_2HPO_4, 0.05 mM EDTA, 5 mM $MgCl_2$, 1 mM ADP, 10 mM glutamate, 2.5 mM malate, 10 mM Tris–HCl pH 7.4 and 1 mg/ml of free fatty acid bovine serum albumin). For *in organello* transcription analysis, 20 μCi of [⟨-^{32}P]-UTP was added and incubated at 37°C for 60 min in a rotary shaker. For pulse chase experiments, mitochondria were preincubated for 2 h with [⟨-^{32}P]-UTP, precipitated by centrifuging at 13 000 r.p.m., and resuspended in fresh incubation medium in the presence of 200-fold excess of cold UTP, and incubated for several periods of time before harvesting. Mitochondrial RNA was extracted by Protease IX (Sigma) digestion and run on methyl-mercury hydroxide agarose gel. The gels were then stained with ethidium bromide, photographed under a UV screen and dried for autoradiography (Phosphorimaging System, Biorad).

Biochemical assays

Specific activities of respiratory chain complexes were measured on tissue homogenates, and normalized to citrate synthase activity, an indicator of the number of mitochondria (58).

Analysis in body fluids

AST, ALT, CK, Creatinine, glucose and urea were determined in blood samples by standard methods. Lactate levels were measured by the Lactate Pro kit (Arkray, Kyoto, Japan). Urinary protein was measured by Bayer Multistix 10 SG Reagent Strips.

Cell cultures

Primary MEF cultures were prepared from individual E13.5 embryos obtained from an intercross of heterozygous Mpv17 mice. MEFs were cultured in complete DMEM with high glucose with or without 10% fetal bovine serum (see Results).

For immunofluorescence analysis, cells were plated on coverslips, preincubated with 100 nM MitoTracker Red dye (Molecular Probes) for 30 min at 37°C, followed by fixation for 20 min with 4% paraformaldehyde in PBS at 37°C, and permeabilized with 0.5% Triton X in PBS for 5 min at room temperature. The cells were then incubated with primary Anti-DNA antibody (Progen) for 1 h (diluition anti-DNA 1:25). After incubation, the cells were rinsed in PBS and primary antibodies were visualized using a fluorescent-tagged secondary antibody (Alexa Fluor 488 goat anti-mouse IgG) at 1:1000 dilution in PBS.

Protein blot analysis

Ten percent w/v homogenates in 10 mM phosphate buffer pH 7.4 were prepared from different tissues and centrifuged at 800*g* for 10 min to eliminate cellular debris. Total protein extracts were run through a 12% SDS–polyacrylamide gel (~40 μg/sample), and electroblotted onto nitrocellulose filters. The filters were immunostained with specific antibodies against complex IV subunit I (COX1) and the 30 kDa subunit of SDH (Molecular probes, Invitrogen) and protein bands were visualized using the ECL chemiluminscence kit (Amersham).

Twenty microgram of proteins from isolated liver mitochondria were run on a 12% SDS–polyacrylamide gel for Mterf1 expression analysis and the nitrocellulose filter was immunostained with a Mterf1 polyclonal antibody (kindly provided by Dr Aleksandra Trifunovic, Karolinska Institute, Stockholm).

Statistics

Two-tailed, unpaired Student's *t*-test was used for statistical analysis. Survival analysis was carried out using the Kaplan–Meier estimate and log-rank test for survival probability.

SUPPLEMENTARY MATERIAL

Supplementary Material is available at *HMG* Online.

REFERENCES

1. Spinazzola, A. and Zeviani, M. (2007) Disorders of nuclear-mitochondrial intergenomic communication. *Biosci. Rep.*, **27**, 39–51.
2. Sarzi, E., Bourbon, A., Chrétien, D., Zarhrate, M., Colcos, J., Slama, A., Cormier-Daire, V., de Lonlay, P., Munnich, A. and Rötig, A. (2007) Mitochondrial DNA depletion is a prevalent cause of multiple respiratory chain deficiency in childhood. *J. Pediatr.*, **150**, 531–534.
3. Saada, A., Shaag, A., Mandel, H., Nevo, Y., Eriksson, S. and Elpeleg, O. (2001) Mutant mitochondrial thymidine kinase in mitochondrial DNA depletion myopathy. *Nat. Genet.*, **29**, 342–344.
4. Mandel, H., Szargel, R., Labay, V., Elpeleg, O., Saada, A., Shalata, A., Anbinder, Y., Berkowitz, D., Hartman, C., Barak, M. *et al.* (2001) The deoxyguanosine kinase gene is mutated in individuals with depleted hepatocerebral mitochondrial DNA. *Nat. Genet.*, **29**, 337–341.
5. Bourdon, A., Minai, L., Serre, V., Jais, J.P., Sarzi, E., Aubert, S., Chrétien, D., de Lonlay, P., Paquis-Flucklinger, V., Arakawa, H. *et al.* (2007) Mutation of RRM2B, encoding p53-controlled ribonucleotide reductase (p53R2), causes severe mitochondrial DNA depletion. *Nat. Genet.*, **39**, 776–780.
6. Nishino, I., Spinazzola, A. and Hirano, M. (1999) Thymidine phosphorylase gene mutations in MNGIE, a human mitochondrial disorder. *Science*, **283**, 689–692.

7. Naviaux, R.K. and Nguyen, K.V. (2004) POLG mutations associated with Alpers' syndrome and mitochondrial DNA depletion. *Ann. Neurol.*, **55**, 706–712.

8. Ferrari, G., Lamantea, E., Donati, A., Filosto, M., Briem, E., Carrara, F., Parini, R., Limonati, A., Santer, R. and Zeviani, M. (2005) Infantile hepatocerebral syndromes associated with mutations in the mitochondrial DNA polymerase-gammaA. *Brain*, **128**, 723–731.

9. Hakonen, A.H., Isohanni, P., Paetau, A., Herva, R., Suomalainen, A. and Lonnqvist, T. (2007) Recessive Twinkle mutations in early onset encephalopathy with mtDNA depletion. *Brain*, **130**, 3032–3040.

10. Sarzi, E., Goffart, S., Serre, V., Chretien, D., Slama, A., Munnich, A., Spelbrink, J.N. and Rotig, A. (2007) Twinkle helicase (PEO1) gene mutation causes mitochondrial DNA depletion. *Ann. Neurol.*, **62**, 579–587.

11. Elpeleg, O., Miller, C., Hershkovitz, E., Bitner-Glindzicz, M., Bondi-Rubinstein, G., Rahman, S., Pagnamenta, A., Eshhar, S. and Saada, A. (2005) Deficiency of the ADP-forming succinyl–CoA synthase activity is associated with encephalomyopathy and mitochondrial DNA depletion. *Am. J. Hum. Genet.*, **76**, 1081–1086.

12. Ostergaard, E., Christensen, E., Kristensen, E., Mogensen, B., Duno, M., Shoubridge, E.A. and Wibrand, F. (2007) Deficiency of the alpha subunit of succinate-coenzyme A ligase causes fatal infantile lactic acidosis with mitochondrial DNA depletion. *Am. J. Hum. Genet.*, **81**, 383–387.

13. Spinazzola, A., Viscomi, C., Fernandez-Vizarra, E., Carrara, F., D'Adamo, P., Calvo, S., Marsano, R.M., Donnini, C., Weiher, H., Strisciuglio, P. *et al.* (2006) MPV17 encodes an inner mitochondrial membrane protein and is mutated in infantile hepatic mitochondrial DNA depletion. *Nat. Genet.*, **38**, 570–575.

14. Wong, L.J., Brunetti-Pierri, N., Zhang, Q., Yazigi, N., Bove, K.E., Dahms, B.B., Puchowicz, M.A., Gonzalez-Gomez, I., Schmitt, E.S., Truong, C.K. *et al.* (2007) Mutations in the MPV17 gene are responsible for rapidly progressive liver failure in infancy. *Hepatology*, **46**, 1218–1227.

15. Navarro-Sastre, A., Martín-Hernández, E., Campos, Y., Quintana, E., Medina, E., de Las Heras, R.S., Lluch, M., Muñoz, A., del Hoyo, P., Martín, R. *et al.* (2008) Lethal hepatopathy and leukodystrophy caused by a novel mutation in MPV17 gene: description of an alternative MPV17 spliced form. *Mol. Genet. Metab.*, **94**, 234–239.

16. Spinazzola, A., Santer, R., Akman, O.H., Tsiakas, K., Schaefer, H., Ding, X., Karadimas, C.L., Shanske, S., Ganesh, J., Di Mauro, S. *et al.* (2008) Hepatocerebral form of mitochondrial DNA depletion syndrome. *Arch. Neurol.*, **65**, 1–6.

17. Karadimas, C.L., Vu, T.H., Holve, S.A., Chronopoulou, P., Quinzii, C., Johnsen, S.D., Kurth, J., Eggers, E., Palenzuela, L., Tanji, K. *et al.* (2006) Navajo neurohepatopathy is caused by a mutation in the *MPV17* gene. *Am. J. Hum. Genet.*, **79**, 544–548.

18. Appenzeller, O., Kornfeld, M. and Snyder, R. (1976) Acromutilating, paralyzing neuropathy with corneal ulceration in Navajo children. *Arch. Neurol.*, **33**, 733–738.

19. Spinazzola, A., Massa, V., Hirano, M. and Zeviani, M. (2008) Lack of founder effect for an identical mtDNA depletion syndrome (MDS)-associated MPV17 mutation shared by Navajos and Italians. *Neuromuscul. Disord.*, **18**, 315–318.

20. Weiher, H., Noda, T., Gray, D.A., Sharpe, A.H. and Jaenisch, R. (1990) Transgenic mouse model of kidney disease: insertional inactivation of ubiquitously expressed gene leads to nephrotic syndrome. *Cell*, **62**, 425–434.

21. O'Bryan, T., Weiher, H., Rennke, H.G., Kren, S. and Hostetter, T.H. (2000) Course of renal injury in the Mpv17-deficient transgenic mouse. *J. Am. Soc. Nephrol.*, **11**, 1067–1074.

22. Clozel, M., Hess, P., Fischli, W., Löffler, B.M., Zwacka, R.M., Reuter, A. and Weiher, H. (1999) Age-dependent hypertension in Mpv17-deficient mice, a transgenic model of glomerulosclerosis and inner ear disease. *Exp. Gerontol.*, **34**, 1007–1015.

23. Meyer zum Gottesberge, A.M., Reuter, A. and Weiher, H. (1996) Inner ear defect similar to Alport's syndrome in the glomerulosclerosis mouse model Mpv17. *Eur. Arch. Otorhinolaryngol.*, **253**, 470–474.

24. Meyer zum Gottesberge, A.M. and Felix, H. (2005) Abnormal basement membrane in the inner ear and the kidney of the Mpv17−/− mouse strain: ultrastructural and immunohistochemical investigations. *Histochem. Cell. Biol.*, **124**, 507–516.

25. Zwacka, R.M., Reuter, A., Pfaff, E., Moll, J., Gorgas, K., Karasawa, M. and Weiher, H. (1994) The glomerulosclerosis gene Mpv17 encodes a peroxisomal protein producing reactive oxygen species. *EMBO J.*, **13**, 5129–5134.

26. Scarpulla, R.C. (2006) Nuclear control of respiratory gene expression in mammalian cells. *J. Cell. Biochem.*, **97**, 673–683.

27. Gleyzer, N., Vercauteren, K. and Scarpulla, R.C. (2005) Control of mitochondrial transcription specificity factors (TFB1M and TFB2M) by nuclear respiratory factors (NRF-1 and NRF-2) and PGC-1 family coactivators. *Mol. Cell. Biol.*, **25**, 1354–1366.

28. Scarpulla, R.C. (2008) Transcriptional paradigms in mammalian mitochondrial biogenesis and function. *Physiol. Rev.*, **88**, 611–638.

29. Zhou, X., Solaroli, N., Bjerke, M., Stewart, J.B., Rozell, B., Johansson, M. and Karlsson, A. (2008) Progressive loss of mitochondrial DNA in thymidine kinase 2-deficient mice. *Hum. Mol. Genet.*, **17**, 2329–2335.

30. Akman, H.O., Dorado, B., López, L.C., García-Cazorla, A., Vilà, M.R., Tanabe, L.M., Dauer, W.T., Bonilla, E., Tanji, K. and Hirano, M. (2008) Thymidine kinase 2 (H126 N) knockin mice show the essential role of balanced deoxynucleotide pools for mitochondrial DNA maintenance. *Hum. Mol. Genet.*, **17**, 2433–2440.

31. Masuyama, M., Iida, R., Takatsuka, H., Yasuda, T. and Matsuki, T. (2005) Quantitative change in mitochondrial DNA content in various mouse tissues during aging. *Biochim. Biophys. Acta*, **1723**, 302–308.

32. Mandel, H., Hartman, C., Berkowitz, D., Elpeleg, O.N., Manov, I. and Iancu, T.C. (2001) The hepatic mitochondrial DNA depletion syndrome: ultrastructural changes in liver biopsies. *Hepatology*, **34**, 776–784.

33. Larsson, N.G., Wang, J., Wilhelmsson, H., Oldfors, A., Rustin, P., Lewandoski, M., Barsh, G.S. and Clayton, D.A. (1998) Mitochondrial transcription factor A is necessary for mtDNA maintenance and embryogenesis in mice. *Nat. Genet.*, **18**, 231–236.

34. Barthelemy, C., Ogier de Baulny, H., Diaz, J., Cheval, M.A., Frachon, P., Romero, N., Goutieres, F., Fardeau, M. and Lombes, A. (2001) Late-onset mitochondrial DNA depletion: DNA copy number, multiple deletions, and compensation. *Ann. Neurol.*, **49**, 607–617.

35. Martin, M., Cho, J., Cesare, A.J., Griffith, J.D. and Attardi, G. (2005) Termination factor-mediated DNA loop between termination and initiation sites drives mitochondrial rRNA synthesis. *Cell*, **123**, 1227–1240.

36. Montoya, J., Christianson, T., Levens, D., Rabinowitz, M. and Attardi, G. (1982) Identification of initiation sites for heavy-strand and light-strand transcription in human mitochondrial DNA. *Proc. Natl Acad. Sci.*, **79**, 7195–7199.

37. Montoya, J., Gaines, G.L. and Attardi, G. (1983) The pattern of transcription of the human mitochondrial rRNA genes reveals two overlapping transcription units. *Cell*, **42**, 151–159.

38. Park, C.B., Asin-Cayuela, J., Cámara, Y., Shi, Y., Pellegrini, M., Gaspari, M., Wibom, R., Hultenby, K., Erdjument-Bromage, H., Tempst, P. *et al.* (2007) MTERF3 is a negative regulator of mammalian mtDNA transcription. *Cell*, **130**, 273–285.

39. Nishimura, E.K., Granter, S.R. and Fisher, D.E. (2005) Mechanisms of hair graying: incomplete melanocyte stem cell maintenance in the niche. *Science*, **307**, 720–724.

40. Mak, S.S., Moriyama, M., Nishioka, E., Osawa, M. and Nishikawa, S. (2006) Indispensable role of Bcl2 in the development of the melanocyte stem cell. *Develop. Biol.*, **291**, 144–153.

41. Tobin, D.J. and Paus, R. (2001) Graying: gerontobiology of the hair follicle pigmentary unit. *Exp. Gerontol.*, **36**, 29–54.

42. Binder, C.J., Weiher, H., Exner, M. and Kerjaschki, D. (1999) Glomerular overproduction of oxygen radicals in Mpv17 gene-inactivated mice causes podocyte foot process flattening and proteinuria: a model of steroid-resistant nephrosis sensitive to radical scavenger therapy. *Am. J. Pathol.*, **154**, 1067–1075.

43. Hagiwara, M., Yamagata, K., Capaldi, R.A. and Koyama, A. (2006) Mitochondrial dysfunction in focal segmental glomerulosclerosis of puromycin aminonucleoside nephrosis. *Kidney Int.*, **69**, 1146–1152.

44. Rötig, A. (2003) Renal disease and mitochondrial genetics. *J. Nephrol.*, **16**, 286–292.

45. Inoue, K., Nakada, K., Ogura, A., Isobe, K., Goto, Y., Nonaka, I. and Hayashi, J.I. (2000) Generation of mice with mitochondrial dysfunction by introducing mouse mtDNA carrying a deletion into zygotes. *Nat. Genet.*, **26**, 176–181.

46. Kimura, T., Takeda, S., Sagiya, Y., Gotoh, M., Nakamura, Y. and Arakawa, H. (2003) Impaired function of p53R2 in Rrm2b-null mice causes severe renal failure through attenuation of dNTP pools. *Nat. Genet.*, **34**, 440–445.

47. Gubler, M.C. (2008) Inherited diseases of the glomerular basement membrane. *Nat. Clin. Pract. Nephrol.*, **4**, 24–37.
48. Reuter, A., Nestl, A., Zwacka, R.M., Tuckermann, J., Waldherr, R., Wagner, E.M., Höyhtyä, M., Meyer zum Gottesberge, A.M., Angel, P. and Weiher, H. (1998) Expression of the recessive glomerulosclerosis gene Mpv17 regulates MMP-2 expression in fibroblasts, the kidney, and the inner ear of mice. *Mol. Biol. Cell*, **9**, 1675–1682.
49. Irwin, W.A., Bergamin, N., Sabatelli, P., Reggiani, C., Megighian, A., Merlini, L., Braghetta, P., Columbaro, M., Volpin, D., Bressan, G.M. *et al.* (2003) Mitochondrial dysfunction and apoptosis in myopathic mice with collagen VI deficiency. *Nat. Genet.*, **35**, 367–371.
50. Angelin, A., Tiepolo, T., Sabatelli, P., Grumati, P., Bergamin, N., Golfieri, C., Mattioli, E., Gualandi, F. and Ferlini, A. (2007) Mitochondrial dysfunction in the pathogenesis of Ullrich congenital muscular dystrophy and prospective therapy with cyclosporins. *Proc. Natl. Acad. Sci.*, **104**, 991–996.
51. Merlini, L., Angelin, A., Tiepolo, T., Braghetta, P., Sabatelli, P., Zamparelli, A., Ferlini, A., Maraldi, N.M., Bonaldo, P. and Bernardi, P. (2008) Cyclosporin A corrects mitochondrial dysfunction and muscle apoptosis in patients with collagen VI myopathies. *Proc. Natl. Acad. Sci.*, **105**, 5225–5229.
52. Heath, K.E., Campos-Barros, A., Toren, A., Rozenfeld-Granot, G., Carlsson, L.E., Savige, J., Denison, J.C., Gregory, M.C., White, J.G., Barker, D.F. *et al.* (2001) Nonmuscle myosin heavy chain IIA mutations define a spectrum of autosomal dominant macrothrombocytopenias: May-Hegglin anomaly and Fechtner, Sebastian, Epstein, and Alport-like syndromes. *Am. J. Hum. Genet.*, **69**, 1033–1045.
53. Lalwani, A.K., Atkin, G., Li, Y., Lee, J.Y., Hillman, D.E. and Mhatre, A.N. (2008) Localization in stereocilia, plasma membrane, and mitochondria suggests diverse roles for NMHC-IIa within cochlear hair cells. *Brain. Res.*, **1197**, 13–22.
54. Sciacco, M. and Bonilla, E. (1996) Cytochemistry and immunocytochemistry of mitochondria in tissue sections. *Meth. Enzymol.*, **264**, 509–521.
55. Cree, L.M., Patel, S.K., Pyle, A., Lynn, S., Turnbull, D.M., Chinnery, P.F. and Walker, M. (2008) Age-related decline in mitochondrial DNA copy number in isolated human pancreatic islets. *Diabetologia*, **51**, 1440–1443.
56. Fernández-Vizarra, E., López-Pérez, M.J. and Enriquez, J.A. (2002) Isolation of biogenetically competent mitochondria from mammalian tissues and cultured cells. *Methods*, **26**, 292–297.
57. Fernández-Vizarra, E., Enriquez, J.A., Pérez-Martos, A., Montoya, J. and Fernández-Silva, P. (2008) Mitochondrial gene expression is regulated at multiple levels and differentially in the heart and liver by thyroid hormones. *Curr. Genet.*, **54**, 13–22.
58. Bugiani, M., Tiranti, V., Farina, L., Uziel, G. and Zeviani, M. (2005) Novel mutations in COX15 in long surviving Leigh syndrome patient with cytochrome c oxidase deficiency. *J. Med. Genet.*, **42**, e28.